

The influence of soft spectral components on the structure and stability of warm absorbers in AGN

Susmita Chakravorty^{1,2,3}*, Ranjeev Misra^{1*}, Martin Elvis^{3*}, Ajit K. Kembhavi^{1*}, Gary Ferland^{4*}

¹*IUCAA, Post Bag 4, Ganeshkhind, Pune 411 007, India;*

²*Astronomy Department, Harvard University, Cambridge, MA 02138, USA;*

³*Harvard-Smithsonian Center for Astrophysics, Cambridge, MA 02138, USA;*

⁴*Department of Physics and Astronomy, University of Kentucky, Lexington, KY 40506, USA.*

27 January 2012

ABSTRACT

The radiation from the central regions of active galactic nuclei, including that from the accretion disk surrounding the black hole, is likely to peak in the extreme ultraviolet $\sim 13 - 100$ eV. However, due to Galactic absorption, we are limited to constraining the physical properties - black hole mass and accretion rate - from what observations we have below ~ 10 eV or above ~ 100 eV. In this paper we predict the thermal and ionization states of warm absorbers as a function of the shape of the unobservable continuum. In particular we model an accretion disk at $kT_{in} \sim 10$ eV and a *soft excess* at $kT_{se} \sim 150$ eV. The warm absorber, which is the highly ionized gas along the line of sight to the continuum, shows signatures in the $\sim 0.3 - 2$ keV energy range consisting of numerous absorption lines and edges of various ions, some of the prominent ones being H- and He-like oxygen, neon, magnesium and silicon. We find that the properties of the warm absorber are significantly influenced by the changes in the temperature of the accretion disk, as well as by the strength of the *soft excess*, as they affect the optical depth particularly for iron and oxygen. These trends may help develop a method of characterising the shape of the unobservable continuum and the occurrence of warm absorbers.

Key words:

1 INTRODUCTION

Accretion of matter onto a supermassive black hole and the conversion of the gravitational energy into radiation, via an accretion disk, is the main source of energy output in active galactic nuclei (AGN). The radiation from AGN is likely to peak in the extreme ultraviolet (EUV) $\sim 10 - 100$ eV (Lynden-Bell 1969; Pringle, Rees & Pacholczyk 1973; Shields 1978; Shakura & Sunyaev 1973; Netzer 1985). However, Galactic absorption of EUV light results in a ‘blind spot’ in the energy range $13 - 100$ eV ($\sim 912 - 50 \text{ \AA}$, marked as “unobserved” in Figure 1) introducing an uncertainty in the shape of the spectral energy distribution (SED) of AGN, just where it is expected to peak. Attempts have been made to reconstruct the SED from observations available below ~ 10 eV and above ~ 100 eV (Siemiginowska et al. 1995; Sobolewska et al. 2004a,b, and references therein). This unobserved part of the SED is most effective at ionizing gas (which is

the very reason it also gets absorbed by the Galaxy). Hence the continuum will influence the intervening line of sight gas, local to the AGN, and the resultant absorption and emission line strengths of the various ions seen in far ultraviolet (FUV) and the Balmer continuum can be used to constrain the SED, as discussed by Netzer (1987).

At the high energy end of the ‘blind spot’, i.e. in the soft X-ray ($0.1 - 10$ keV), observations of most AGN reveal that, for a majority, the SED from $2 - 10$ keV is well approximated by a power-law $f(\nu) \sim \nu^{-\alpha}$ with spectral indices ~ 0.8 . The join between the EUV (2500 \AA) and the soft X-ray (2 keV), α_{OX} , is steeper, with typical values of ~ 1.2 for Seyfert 1 galaxies (Netzer 1993). Hence extending the X-ray power-law to the ultraviolet (UV) cannot explain the observed flux (but see Laor (1997)). An ionizing continuum with two power-law components, a steep one for the join between EUV and soft X-ray, and a flatter one for the soft X-ray SED, can represent the overall shape of the AGN spectra in the energy range $3 \text{ eV} - 2 \text{ keV}$.

However, such an SED is not a physical model and does not resemble certain specific features expected in this energy range. In particular, the proposed accretion disk, whose in-

* E-mail: schakravorty@head.cfa.harvard.edu (SC);
rmisra@iucaa.ernet.in (RM); akk@iucaa.ernet.in (AK);
elvis@head.cfa.harvard.edu (MA); gary@pa.uky.edu (GF)

nermost stable orbit should have a temperature of ~ 13 eV, for a black hole of mass $10^8 M_\odot$ and an accretion rate of $\dot{m}/\dot{m}_{Edd} = 0.1$ (Shakura & Sunyaev 1973; Frank, King & Raine 2002), is not included. Another spectral component which would remain unaccounted for by a simple two power-law continuum is the *soft excess* which is seen in most AGN below 2 keV. The *soft excess* could be a Comptonised disk component (Czerny & Elvis 1987), an additional quasi-blackbody (Crummy et al. 2006; Korista, Ferland & Baldwin 1997; Ross & Fabian 1993, 2005) or due to relativistic broadened absorption features (Gierlinski & Done 2004). Such spectral components are likely to have important effects on the nature of the absorbing gas along the line of sight towards the central engine of the AGN.

In the 0.3 - 1.5 keV soft X-ray spectra of about half of all Seyfert 1 galaxies (Nandra & Pounds 1994; Reynolds 1997; George et al. 1998) and quasars (Piconcelli et al. 2005) one can find signatures of photoionized gas called “warm absorbers” (hereafter WAs, Halpern (1984)). These signatures are, often, absorption lines and edges from highly ionized species, such as OVII, OVIII, FeXVII, NeX, CV and CVI (Collinge et al. 2001; Kaastra et al. 2002; Kinkhabwala et al. 2002; Blustin et al. 2003; Krongold et al. 2003; Netzer et al. 2003; Turner et al. 2004). The typical column density observed for the gas is $N_H \sim 10^{22 \pm 1} \text{ cm}^{-2}$. The ionization parameter ξ of the WA spans a range $\sim 10 - 1000 \text{ erg cm s}^{-1}$ corresponding to gas temperatures of $10^4 - 10^{6.5} \text{ K}$. Some authors claim that the WA is made up of discrete thermodynamic phases in near pressure equilibrium (Andrade-Velazquez et al. 2010, and references therein), while others (Ogle et al. 2004; Steenbrugge et al. 2005; Behar 2009) believe that the gas has a continuous distribution of temperature and pressure.

In this temperature range heating and cooling processes are respectively dominated by photoionization and recombination of higher ionization states of heavier elements. These processes result in local regions of thermal stability in this otherwise unstable temperature range (Krolik et al. 1981; Gehrels & Williams 1993; Hess et al. 1997). Chakravorty et al. (2009) showed that the nature of the WA is strongly influenced by the chemical composition of the absorbing gas. It was shown that the abundance of iron and oxygen, which have important atomic transitions in the sub-keV energy range are particularly important.

To obtain the equilibrium conditions for a gas with an assumed set physical conditions, we have used the publicly available photoionization code CLOUDY¹ version C07.02 (hereafter C07), see Ferland (1998). CLOUDY calculates the ionization equilibrium conditions by solving the energy and charge conservation equations under the assumption that all the atomic processes have had time to reach a steady state. Any stable photoionised gas will lie on the thermal equilibrium curve (hereafter referred to as the *stability curve*) where heating balances cooling. The stability curve of temperature (T) against pressure (ξ/T), where ξ is the ionization parameter (see below for definition), is often used to study the nature of the WA. Gas lying off the stability curve will heat or cool until reaching the curve. If the curve has kinks that produce multiple stable values at fixed ξ/T , then the WA can have multiple temperature phases in pressure equilibrium. The shape of the stability curve depends on the SED of the ionizing continuum and the chemical abundance of the gas (Reynolds & Fabian

1995; Krolik & Kriss 2001; Komossa & Meerschweinchen 2000; Komossa & Mathur 2001; Chakravorty et al. 2008, 2009).

In this paper we investigate the behaviour of the stability curve as a function of the *disk blackbody* and *soft excess* both to understand the role of these spectral components on the nature of the WA, and to examine whether the observable parameters of the WA can diagnose the shape of the AGN continuum in the EUV ‘blind spot’. In Section 2 we describe the different models of the AGN continuum that we are interested in and use these SEDs to study their effect on the stability curves in Section 3. We investigate the causes of the variations in the stability curves in Section 4 by studying the heating and ionization fractions of the elements and ions which are responsible for determining the nature of the WA. Section 5 examines the relevance of a few other physical parameters, like the X-ray slope of the ionizing continuum and the abundance of the absorbing gas, (also discussed in Chakravorty et al. 2009) in the context of the present study. The multi-phase nature of the WA is discussed in Section 6 and we conclude our results in Section 7.

2 THE AGN CONTINUUM

The 2 - 10 keV X-ray spectra of most of the observed active galactic nuclei (AGN) can be modeled satisfactorily using a power-law $f(\nu) \sim \nu^{-\alpha}$ where the spectral index α for most AGN lie in the range $0.7 < \alpha < 0.9$ (Wilkes & Elvis 1987; Grupe et al. 2006; Lopez et al. 2006). The optical depth $\tau = 1$ for photons at 0.2 keV with a typical Galactic hydrogen column density of $N_H = 3 \times 10^{20} \text{ cm}^{-2}$. Extinction is a steeply rising function of column density, e.g. $\tau = 2$ at 0.2 keV for $N_H = 5 \times 10^{20} \text{ cm}^{-2}$. Thus, we lack observational constraints on the evolution of the X-ray power-law at lower energies. However, for most AGN, the UV flux is found to be much higher than what a simple extrapolation of the X-ray power-law to lower energies would predict (Elvis et al. 1994; Zheng et al. 1997; Shang et al. 2005), but see Laor (1997) for exceptions. The slope α_{OX} , defined as

$$\alpha_{OX} = -0.384 \log \left[\frac{f(2 \text{ keV})}{f(4.7 \text{ eV} = 2500 \text{ \AA})} \right] \quad (1)$$

by Tananbaum et al. (1979), is conventionally used to parametrize the nominal power-law between the UV and soft X-ray bands. The observed range is $1 \lesssim \alpha_{OX} \lesssim 2$ (Stalin et al. 2009; Green et al. 2009, and references therein).

The overall shape of the AGN continuum in the energy range of $\sim 4.7 \text{ eV} (2500 \text{ \AA}) - 10 \text{ keV}$ can, thus, be represented as a sum of two power-law components

$$f(\nu) \sim [\nu^{-\alpha} + A_1 \nu^{-\alpha_s}] e^{-\frac{\nu}{\nu_{max}}}, \quad \text{for } E(= h\nu) \geq 4.7 \text{ eV}, \quad (2)$$

where $\alpha_s (> 0)$ is the spectral index of a steep soft component and A_1 is the relative normalization factor to realize the desired values of α_{OX} (dotted-and-dashed curve in Figure 1.). Chakravorty et al. (2009) had used such an SED with $E_{max} = h\nu_{max} = 200 \text{ keV}$, and this value is maintained throughout this paper, as well. Results from the Swift/BAT (Burst Alert Telescope) hard X-ray sky survey (Tueller et al. 2008) show that, of the brightest few dozen AGN, for which E_{max} can be determined, the cut-off spans the range 50 to 450 keV. In Chakravorty et al. (2009) we have shown that in the range $50 \text{ keV} < E_{max} < 400 \text{ keV}$, the variation in E_{max} does not have any significant effect on the nature of the warm absorber. For energies lower than 4.7 eV Chakravorty et al. (2009) followed the cut-off scheme

$$f(\nu) \sim \nu^{-0.5} \quad \text{for } 2.8 \leq E(= h\nu) < 4.7 \text{ eV}$$

¹ URL: <http://www.nublado.org/>

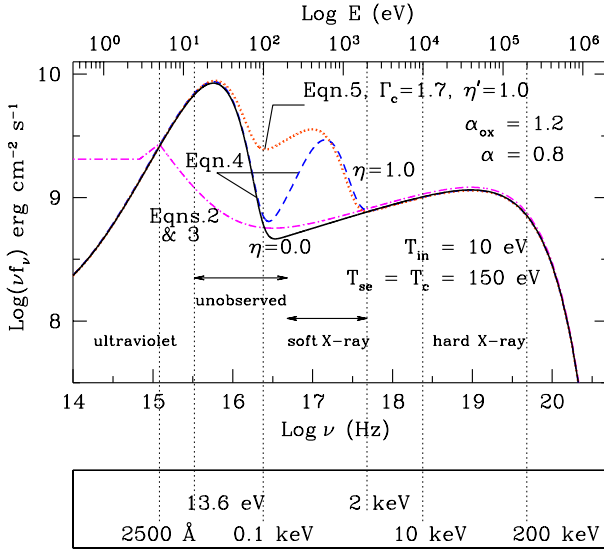


Figure 1. Comparison between various ionizing continua : the broken power-law (Equation 2, dotted-and-dashed line) and more realistic SEDs having *disk blackbody* and *soft excess* components (Equations 4 and 5). For all the curves $\alpha = 0.8$ and $\alpha_{OX} = 1.2$. Using Equation 4 we draw the solid curve with $\eta = 0.0$ and the dashed curve with $\eta = 1.0$, while the dotted curve is drawn using Equation 5 with $\eta' = 1.0$. The temperature of the innermost ring of the accretion disk is $T_{in} = 10$ eV and temperature corresponding to the *soft excess* is $T_{se} = T_c = 150$ eV. See text for further details.

$$\begin{aligned} &\sim \nu^{-1.0} \text{ for } 0.12 \leq E(=h\nu) < 2.8 \text{ eV} \\ &\sim \nu^{2.5} \text{ for } E(=h\nu) < 0.12 \text{ eV} \end{aligned} \quad (3)$$

This scheme is similar to that described by Mathews & Ferland (1987). However, a SED described by Equations 2 and 3 may sometimes be an inadequate description for the AGN ionizing continuum because it fails to represent the signature of the accretion disk at ~ 10 eV or the *soft excess* component.

2.1 Disk blackbody

Multiwavelength observations suggest that the AGN continua peak in the EUV energy band and emission here usually dominates the quasar luminosity (Neugebauer et al. 1979; Shields 1978; Malkan & Sargent 1982; Elvis et al. 1986; Czerny & Elvis 1987; Mathews & Ferland 1987; Laor et al. 1990; Siemiginowska et al. 1995; Zheng et al. 1997; Sobolewska et al. 2004a,b). This spectral component, often referred to as the “Big Blue Bump”, is considered to be the signature of the presence of an accretion disk as discussed by Lynden-Bell (1969); Pringle, Rees & Pacholczyk (1973); Shields (1978); Shakura & Sunyaev (1973).

According to the standard theory of accretion disks by Shakura & Sunyaev (1973), the emission from the disk can be modeled as a sum of local blackbody radiations emitted from annuli of the disk at different radii. The temperature of all the subsequent rings can be estimated from the theory if the temperature T_{in} of the innermost ring of the accretion disk is known, which in turn is related to the one-fourth power of the mass of the central black hole and to the fourth power of its accretion rate. Thus for the same accretion rate, T_{in} changes by only a factor of 3 while the black hole mass spans a range of about two order of magnitude. As

such, the resultant shape of the “Big Blue Bump” peaks between $\sim 10 - 100$ eV for the range of black hole masses and accretion rates typical of Seyfert galaxies.

Studies of high redshift quasars show that their UV-EUV SEDs are consistent with the standard theory of accretion disks (Bechtold et al. 1994; Page et al. 2004a,b; Shang et al. 2005). However, typically, the quasars have higher mass ($10^8 \lesssim M_{BH} \lesssim 5 \times 10^{10} M_{\odot}$ Shang et al. 2005; Bechtold et al. 1994) and higher accretion rates (Bechtold et al. 1994). Thus, for the same accretion rates, we can expect the “Big Blue Bump” in quasars to be peaking at lower energies than that in Seyferts which would typically result in steeper $\alpha_{OX} \sim 1.8$ (Bechtold et al. 1994) for the quasars, as compared to 1.2 (Netzer 1993) for the Seyferts.

A standard model for the spectral component from the accretion disk is available as *disk blackbody* (Mitsuda et al. 1984; Makishima et al. 1987) in XSPEC² (Arnaud 1996). We have used version 11.3 of XSPEC to generate the *disk blackbody* spectral component $f_{ddb}(\nu)$ to be used in the construction of the realistic AGN continuum (the third term in Equations 4 and 5). The solid black line in Figure 1 shows a SED which includes a “Big Blue Bump” with $T_{in} = 10$ eV. In this paper we explore “Big Blue Bumps” in the range $10 \leq T_{in} \leq 30$ eV corresponding to $10^{8.47} \leq M_{BH} \leq 10^{6.56} M_{\odot}$ for an accretion rate of $\dot{m}/\dot{m}_{Edd} = 0.1$. This range of accretion disks parameters pertain to Seyfert galaxies or low mass and low accretion rate quasars. We do not explore the parameter range for higher mass quasars because for them T_{in} would move to lower energies and such *disk blackbodies* are less likely to influence the nature of the WA.

2.2 Soft excess

X-ray observations of AGN with ROSAT and XMM-Newton often show that if the 1 - 10 keV power-law is extended to lower energies to fit the observed spectra of type 1 AGN, some unaccounted for excess intensity is usually seen at $E < 1$ keV (Elvis, Wilkes & Tananbaum 1985; Brinkmann 1992; Buehler et al. 1995; Pounds & Reeves 2002). This excess has come to be known as the *soft excess* component. A blackbody with temperature $T_{se} \sim 100 - 200$ eV (i.e. peaking at $\sim 282 - 564$ eV) is often a good fit to the *soft excess* (Matsumoto et al. 2004; Piconcelli et al. 2005; Porquet et al. 2004; Vignali et al. 2004, and references therein). The same authors show that the ratio of the *soft excess* luminosity to power-law luminosity, usually between 0.1 - 10 keV varies from object to object from 0.04 in Mkn 304 (Piconcelli et al. 2005) to $\gtrsim 1.0$ in Ark 564 (Vignali et al. 2004). The simple ‘sum of blackbodies’ model for the accretions disk is a satisfactory qualitative representation of the UV SED with a range of parameter values to cover the observed AGN properties. However, all AGN disks, having supermassive black-holes at their centres, are too cold to reach soft X-rays at ~ 0.5 keV. More sophisticated modifications of this model (Czerny & Elvis 1987; Korista, Ferland & Baldwin 1997) or an additional spectral component is required to explain the *soft excess*.

2.2.1 Blackbody soft excess

A theoretical representation of the *soft excess* as a blackbody is a simplified version of the Ross & Fabian (1993, 2005) model for the *soft excess* component which owes its origin to the reflection

² <http://heasarc.gsfc.nasa.gov/docs/xanadu/xspec/>

of the power-law component of the AGN spectrum from the accretion disk. Thus, in this model the X-ray power-law photons are reprocessed, instead of the ones from the accretion disc.

The general SED for the ionizing continuum including a blackbody *soft excess* component can be given as

$$f(\nu) \sim \left[\{ \nu^{-\alpha} + \eta \frac{2\pi h}{c^2} \frac{\nu^3}{\exp(h\nu/k_B T_{se}) - 1} \} + A_2 f_{dbb}(\nu, T_{in}) \right] e^{-\frac{\nu}{\nu_{max}}}. \quad (4)$$

The first term in the above equation represents the X-ray power-law with spectral index α . The second term is the *soft excess* component, as a blackbody distribution of photons where $T_{se} = 150$ eV is the temperature of the blackbody and η determines the ratio of luminosity in the *soft excess* component to that in the power-law between 0.1 - 10 keV. The third term in Equation 4 is the *disk blackbody* component which is parametrised by T_{in} , the temperature of the innermost ring of the accretion disk. A_2 is the normalisation factor to attain the desired value of α_{OX} . Unless otherwise mentioned, throughout this paper, we have used $\alpha = 0.8$ and $\alpha_{OX} = 1.2$, $E_{max} = h\nu_{max} = 200$ keV. For numerical convenience we put a cut-off for $f(\nu)$ at $E = h\nu = 0.12$ eV below which the flux drops off as $\nu^{2.5}$.

In Figure 1 both, the black solid SED and the blue dashed SED are drawn using Equation 4. For both SEDs, $T_{in} = 10$ eV so that the peak of the diskblackbody lies at ~ 30 eV. The solid line represents a SED which does not have any *soft excess* component, i.e., $\eta = 0$. On the other hand, the blue dashed SED with $\eta = 1.0$ has a moderately strong *soft excess*. See further discussions in Section 3.3.1

2.2.2 Comptonisation by ~ 150 eV plasma

Korista, Ferland & Baldwin (1997) discuss the puzzle that many quasars which show soft ionizing continuum, would have an insufficient number of photons at the 54.4 eV He II edge to generate the observed strength of He II emission seen in the same objects. To explain the strength of the He II line in Mrk 335, Korista, Ferland & Baldwin (1997) invoked a “double peaked” UV-EUV continuum where the second “bump” peaks at ~ 54 eV and contains energy comparable to the classical UV bump at lower energies (~ 10 eV). The

A model, where the photons from the accretion disk are up-scattered by inverse Comptonization due to energetic electrons, does a better job of qualitatively satisfying the required strength of the UV-EUV SED for objects like Mrk 335. Czerny & Elvis (1987) have shown that the models which account for the electron scattering of the accretion disk photons are better than the simple ‘sum of blackbodies’ model. Similar thermal Comptonization models have been worked out by Lightman & Zdziarski (1987); Coppi (1992); Haardt (1993); Coppi (1999) and Beloborodov (1999) among others.

The thermal Comptonization model of Lightman & Zdziarski (1987) has been used by Zdziarski et al. (1996) and extended by Zykli (1999) and their model is included in XSPEC 12.5 (Arnaud 1996) as *nthcomp*. We have used *nthcomp*, where we have assumed that the seed photons coming from the accretion disk (modeled as *disk blackbody*) are reprocessed by the thermal plasma to generate sufficient photons at sub-keV to mimic the *soft excess*, usually observed in AGN. The high energy cut-off for the resulting *soft excess* feature is parametrised by the electron temperature T_c , whereas the low energy rollover is dependent on the effective temperature of

the seed photons from the accretion disk, which in this case is parametrised by T_{in} . Between the low and high energy rollovers the shape of the spectrum is not necessarily a power law, but can be parametrised by an asymptotic power law index Γ_c which would physically be determined by the combination of electron scattering optical depth and electron temperature, i.e. by the Compton y-parameter (Rybicki & Lightman 1986). Beloborodov (1999) had shown that there is a simple relation $\Gamma_c \approx \frac{9}{4}y^{-2/9}$ between the power-law index and the Compton y-parameter. Thus, in our model, Γ_c , used as an input, gives a measure of the extent of Compton reprocessing; i.e. larger the value of Γ_c , lesser is the number of photons reprocessed from the *disk blackbody* component to the high energy photons at $\sim T_c$.

The SED with this alternative model for the *soft excess* $f_c(\nu)$, generated by *nthcomp*, can be written as

$$f(\nu) \sim \left[\{ \nu^{-\alpha} + \eta' f_c(\nu, T_{in}, T_c, \Gamma_c) \} + A_2 f_{dbb}(\nu, T_{in}) \right] e^{-\frac{\nu}{\nu_{max}}}, \quad (5)$$

where η' is the ratio of luminosity of the *soft excess* component for $E (= h\nu) \geq 0.3$ keV to the luminosity of the power-law component in the energy range 0.1 - 10 keV. The orange dotted curve in Figure 1 is drawn using Equation 5 with $T_{in} = 10$ eV, $T_c = 150$ eV $\eta' = 1.0$ and $\Gamma_c = 1.7$. Note that at $E = 54.4$ eV (i.e. $\log \nu = 16.12$) the orange dotted SED has 1.4 times higher flux than the blue dashed SED due to a blackbody *soft excess* and this factor grows to 13.1 at $E = 100$ eV. Thus SEDs like the orange dotted line are better suited to explain observations of objects like Mrk 335 or Mrk 478. See further discussions on this issue in Section 3.3.2.

Chakravorty et al. (2009) showed that the WA temperature range, $10^{4.5} < T < 10^{6.5}$ K, is strongly influenced by the chemical composition of the absorbing gas, particularly by the abundance of iron and oxygen which have important atomic transitions in the sub-keV energy range where the *soft excess* component is likely to have maximum effect. In the following sections we shall extensively investigate the effect of a SEDs, given by Equations 4 and 5, on the nature of the WA, as a function of the shape of the accretion disk component parametrised by the value of T_{in} , and the strength of the *soft excess* feature parametrised by η or Γ_c and η' .

3 STABILITY CURVES ANALYSIS

Studies of WA variability in response to continuum changes show that it is reasonable to assume the WA to be in ionization and thermal equilibrium as observed for NGC 985 (Krongold et al. 2005a), NGC 3783 (Krongold et al. 2005b), NGC 5548 (Andrade-Velazquez et al. 2010). The thermal and ionization equilibrium is governed by heating due to photoionization and cooling due to line emission and collisional recombination (radiative and dielectronic).

We model the WA as an optically thin, plane parallel slab of Solar metallicity gas (as given by Allende Prieto et al. (2001, 2002) for C and O, by Holweger (2001) for N, Ne, Mg, Si and by Grevesse & Sauval (1998) for the remainder of the first thirty elements) with column density $N_H = 10^{22}$ cm $^{-2}$. The absorbing gas is assumed to be illuminated by an ionizing continuum given by Equation 4 or Equation 5 and the ionization state of the gas can be described by specifying the ratio of the ionizing photon flux to the gas density through an *ionization parameter* (see Equation 6).

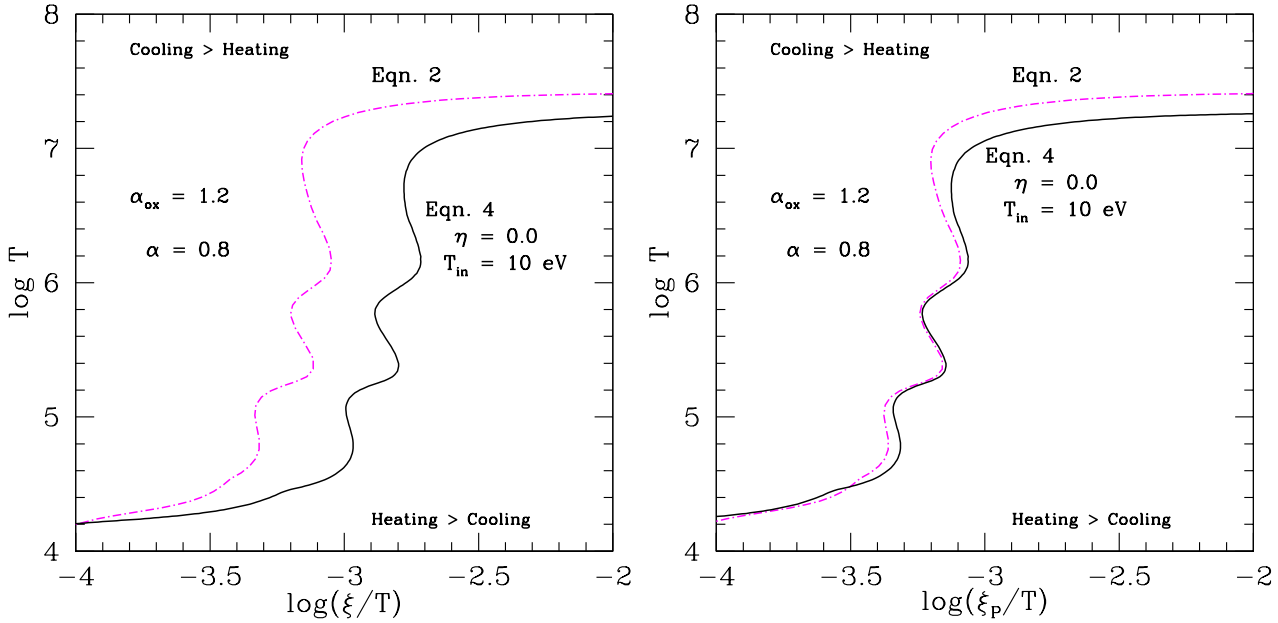


Figure 2. Stability curves demonstrating the advantage of using ξ_P as compared to ξ . The dotted-and-dashed stability curves in both the panels are drawn using the broken power-law continuum (Equation 2), whereas the solid ones are generated for a SED given by Equation 4 with $\eta = 0.0$ and $T_{in} = 10$ eV. Curves drawn with ξ (left panel) are separated in the phase space even if the WA in both the cases have similar nature. On the other hand, the curves drawn using the alternative definition, ξ_P , of the ionization parameter (right panel), are almost identical showing the true nature of the WAs. See text in Section 3.1 for further details.

3.1 Normalising the ionisation parameter

The photoionization state of the WA can be parametrised by the ionization parameter which is the ratio of the ionizing photon flux to the gas density (Tarter, Tucker & Salpeter, 1969):

$$\xi = L_{ion}/n_H R^2 = \int_{h\nu_0=13.6 \text{ eV}}^{13.6 \text{ keV}} \frac{L_\nu}{n_H R^2} d\nu \quad [\text{erg cm s}^{-1}], \quad (6)$$

where L_{ion} is the luminosity between 13.6 eV – 13.6 keV (i.e $1 - 10^3$ Rydberg). Hence $\xi/T \sim L/pR^2$, p being the gas pressure in the WA.

This definition has a certain drawback which is demonstrated by the stability curves on the left panel of Figure 2. The dotted-and-dashed curve is for a gas illuminated with the broken power-law ionizing continuum (Equation 2) and the solid curve is generated with a more realistic SED given by Equation 4 having an accretion disk component with $T_{in} = 10$ eV, but no *soft excess* ($\eta = 0.0$). From Figure 1 we can see that the SED including the accretion disk component (the solid black line) has ~ 50 times more photons at 13.6 eV (1 Rydberg) than the dotted-and-dashed spectra (Equation 2), although they have similar flux at 100 eV. This would result in very different values of ξ in the two cases but very similar WAs, since the WA properties are determined by the photon distribution in soft X-ray ($E \gtrsim 100$ eV) and not by photons with energy $E \ll 100$ eV. The *kinks* in any stability curve are a result of the interplay between the various heating and cooling agents responsible for maintaining the gas at a state of thermal equilibrium (Chakravorty et al. 2008, 2009). The stability curves on the left panel of Figure 2 have almost identical shape for $4.4 < \log T < 6.5$, indicating that they have WAs with identical thermal properties and state of ionization. However, they are separated from each other, by a mere horizontal shift in $\log(\xi/T)$ because of the different ξ values predicted by the two different SEDs. Thus, ξ is a relatively poor parametrization of the nature of the WA. Such a problem with the standard definition of the ionization parameter has been acknowledged by other authors as well. For example, Chelouche & Netzer (2005, and references therein) use an ionization parameter U_x which considers the ionizing flux only between 540 eV to 10 keV.

To circumvent this problem we use a normalisation scheme, appropriate for this paper, as described in the following. All the SEDs considered in this paper (except for ones in Section 5.1) have a common power-law in addition to the diskblackbody and/or the *soft excess* component. Hence we define

$$\xi_P = \frac{L_P}{n_H R^2} = \frac{1}{n_H R^2} \left[4\pi R^2 \int_{h\nu_0=13.6 \text{ eV}}^{200 \text{ keV}} \nu^{-\alpha} d\nu \right] \quad (7)$$

where L_P is a constant luminosity due to the soft X-ray power-law component $f(\nu) \sim \nu^{-\alpha}$ (with $\alpha = 0.8$) in the energy range $E = h\nu = 13.6 \text{ eV} - 200 \text{ keV}$. Thus, ξ_P is the ratio of the ionizing flux, due only to the power-law component in the energy range 13.6 eV to 200 keV, to the gas density. For any SED given by Equations 2, 4 or 5 there would be a unique factor ξ/ξ_P for the same $n_H R^2$. The stability curves corresponding to the ionizing continua given by Equations 2, 4 or 5 are calculated by CLOUDY taking the entire SEDs into account, following which their x-axis ($\log(\xi/T)$) is divided by the unique (to each SED) factor ξ/ξ_P generating a normalised stability curve in the $\log T - \log(\xi_P/T)$ plane. The advantage of such a normalisation is shown in the right panel of Figure 2, where the stability curves overlap closely, demonstrating the true physical scenario of two very similar WAs. Note that these

are the same stability curves which are separated by the horizontal shift in the left panel, as discussed above. This normalisation scheme is used for all subsequent figures in the paper except for Figure 9. In addition to the SEDs which determine the physics of the respective stability curves, the top panels of Figures 3, 4 and 5 also include the constant power-law component (magenta, long-and-short-dashed curve) which is used to normalise the stability curves so that they can be plotted in terms of $\log(\xi_P/T)$.

It is to be noted that while calculating the thermal and ionization properties of the WA, CLOUDY uses the entire SEDs, including all three spectral components (namely the *disk blackbody*, the *soft excess* and the X-ray power-law), described by Equations 4 and 5. The introduction of ξ_P and normalisation of the stability curves is only for the convenience of demonstration of the stability curves and their associated properties. Use of ξ_P merely introduces an overall horizontal shift in these distributions. Further, note that any given range in $\log(\xi/T)$ would correspond to an exactly equal range in $\log(\xi_P/T)$ and vice versa.

3.2 Disk-blackbody

The top panel of Figure 3 shows the ionizing continua which include the *disk blackbody* and the power-law components ($\eta = 0$, Equation 4). As T_{in} is increased from 10 eV to 30 eV, the peak of the flux distribution moves from $\sim 30 - 90$ eV. Photons at $E \lesssim 90$ eV affect only the lower ionization species of the absorbing gas. The resulting WA should show differences only in the nature of the lower ionization phases, and should have very similar higher ionization states. We shall discuss this issue further in Section 4.

Corresponding stability curves are shown in the bottom panel of Figure 3. A hotter *disk blackbody* lowers the Compton temperature branch and increases the temperature of the bottom branch. However, in the $5 < \log T < 6.5$ K temperature range the WAs, the stability curves are independent of the value of T_{in} , i.e., unaffected by the spectral component due to the accretion disk. However, the lower temperature ($\log T < 5$) part of the stability curves undergo remarkable changes with the increase in T_{in} ; for the same value of ξ_P , the gas attains a higher temperature, the stability curve becomes more stable and any possibility of multi-phase existence with higher ionization states is lost. See Section 6 for further discussion on this issue.

3.3 Soft excess

3.3.1 Blackbody soft excess

The top panel of Figure 4 shows the ionizing continua given by Equation 4 with values of $\eta = 0.0, 1.0, 3.0$, representing increasing strengths of the *soft excess* component for a fixed value of the blackbody temperature $T_{se} = 150$ eV. The corresponding stability curves in the bottom panel show a remarkable enhancement of the stable $\log(\xi_P/T)$ range from ~ 0.20 through 0.41 to 0.63 dex for the 10^5 K absorber, as the strength of the *soft excess* is increased from $\eta = 0.0$ through 1.0 to 3.0 . The 10^6 K phase remains unchanged through the variation of η . In the $\eta = 3.0$ case however, the transition from the $\sim 10^5$ to 10^6 K phase is smooth i.e. with no distinct unstable region separating the two temperature regimes. Such a result implies that stronger the *soft excess* component in the spectra, greater is the probability of finding a $\sim 10^5$ K absorber, since the stable region then becomes less susceptible to luminosity variations in the AGN. However, the possibility of the

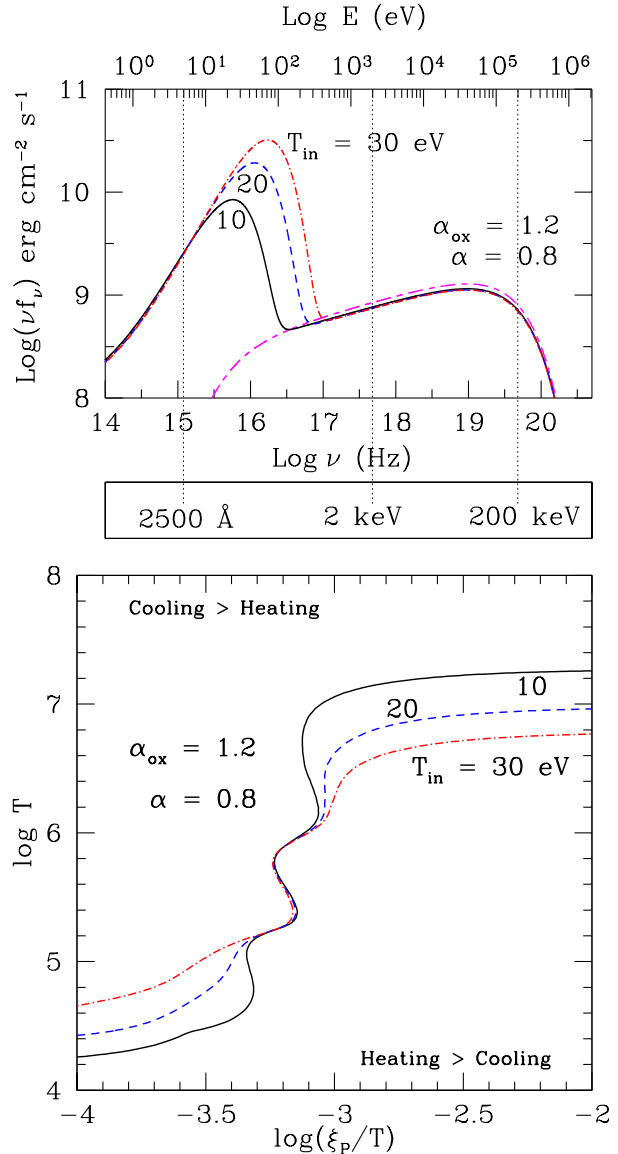


Figure 3. The SEDs in the top panel are constituted by two spectral components, a X-ray power-law and a EUV *disk blackbody*. The curves are for different values of the temperature T_{in} of the innermost ring of the accretion disk. $\alpha = 0.8$ and $\alpha_{OX} = 1.2$ for all the SEDs. We have included the constant power-law (magenta, long-and-short-dashed curve) which is used to normalise the stability curves so that they can be plotted in terms of $\log(\xi_P/T)$. Important energy values including the upper energy cut-off ($E_{max} = 200$ keV) and the range of definition for α_{OX} (2500\AA and 2 keV) have been marked and labeled. The bottom panel shows the stability curves corresponding to the ionizing continua shown in the top panels.

10^5 K gas being in pressure equilibrium with the other WA phases is significantly reduced. We shall return to these points in Section 6.

To find a typical value of η implied by X-ray observations of AGN we refer to two examples, namely a typical Seyfert 1 galaxy NGC 5548 and a narrow line Seyfert 1 galaxy IRAS13349+2438. Andrade-Velazquez et al. (2010) analysed the 800 ks Chandra grating spectra of NGC 5548 and their best fit parameters for the soft X-ray continuum is a power-law with $\alpha = 0.6$ and a blackbody with $T_{se} = 110$ eV. The relative normalisation of the two com-

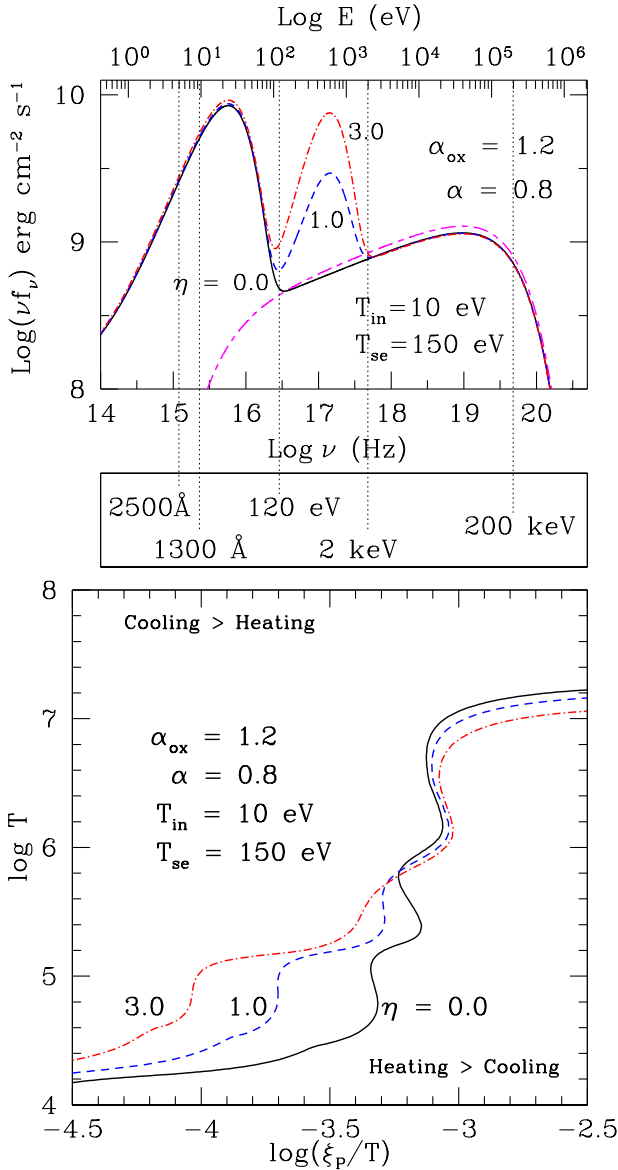


Figure 4. *Top panel* : SEDs which have a *soft excess* component described by a blackbody distribution (see Equation 4) with temperature $T_{\text{se}} = 150 \text{ eV}$. The different SEDs are for different values of η , i.e., for different strengths of the *soft excess* component. $\alpha = 0.8$ and $\alpha_{\text{OX}} = 1.2$ for all the SEDs. The magenta, long-and-short-dashed curve is the same as in the top panel of Figure 3. We have included the energy values 1300 Å and 120 eV to guide the eye in the context of observations of Mrk 478 (see text in Section 3.3.2) *Bottom panel* : The stability curves corresponding to the ionizing continua shown in the top panels. With the growing strength of the *soft excess* component, there is significant increase in the range of ξ_P over which thermally stable warm gas at $\sim 10^5 \text{ K}$ can exist.

ponents results in $\eta \sim 1.2$. Similarly, Holczer et al. (2007) have analysed the 300 ks *Chandra* data for IRAS13349+2438 and have reported the spectral parameters for the best-fit ionizing continuum comprising of a X-ray power-law with $\alpha = 0.9$ and a blackbody with $T_{\text{se}} = 105 \text{ eV}$. From their results we calculate η to be ~ 2.58 . In both cases the values of η is well within the range considered here (0 - 3).

The T_{se} , observed for a large number of type I AGN, lies in

the small range 100 – 200 eV. We have checked whether the influence of the *soft excess* component is modified when the blackbody temperature is varied across this range. Results showed that the stability curves remain unaffected by such variations, e.g. the range in $\text{log}(\xi_P/T)$ for the stable 10^5 K gas changes by merely 0.06 dex as T_{se} varies from 100 eV to 200 eV.

3.3.2 Comptonised soft excess

The blackbody *soft excess* sometimes turns out to be inadequate in explaining the observations. For example, the SED for Mrk 478 may be 1-3 times brighter in νL_ν at $E \sim 120 \text{ eV}$ than it is at 1300 Å ($\sim 10 \text{ eV}$) (Gondhalekar et al. 1994; Marshall et al. 1996). We find that a blackbody *soft excess* cannot satisfy such a condition even with a relatively high normalisation of $\eta = 3.0$ (top panel, Figure 4). We want to investigate if the alternative description of the *soft excess* component, namely the *soft excess* due to thermal Comptonisation, can account for a SED similar to that seen in Mrk 478, and to see what are its effect on the WA.

Spectra generated by Equation 5 with fixed values of $T_c = 150 \text{ eV}$, $T_{\text{in}} = 10 \text{ eV}$ and $\eta' = 1.0$ are drawn in the top panel of Figure 5 for different values of Γ_c . For comparison, we have also drawn the continuum with no *soft excess* (Figure 5 solid curves). The continuum with $\Gamma_c = 2.0$ satisfies the conditions required by observations of Mrk 478 as mentioned by Korista, Ferland & Baldwin (1997).

The influence of a thermal Comptonisation *soft excess* component on the stability curves is shown in the bottom panel of Figure 5. We see again, that the range of $\text{log}(\xi_P/T)$ for the stable 10^5 K branch is increased in width from ~ 0.2 dex to 0.48 dex as η' goes from 0 to 1.0, independent of the value of Γ , facilitating the presence of a stable WA at these temperatures and that the different phases of the WA lose the possibility of existing in pressure equilibrium as the strength of the soft excess component is increased.

The thermal Comptonised and the blackbody models of the *soft excess* result in similar WAs. For example, $\eta = 1.0$ curve (dashed; lower panel of Figure 4) have stable ranges of $\text{log}(\xi_P/T)$ at 10^5 and 10^6 K similar to that of the $\eta' = 1.0$ curves (the dotted and the long-dashed for $\Gamma = 1.7$ and 2.0 respectively; lower panel of Figure 5). The stability curves with $\eta' = 1.0$ do have a slightly smoother rise from the $\sim 10^{4.2}$ to 10^5 K with no distinct intermediate unstable phase, because they have more flux in the $E = 10 - 100 \text{ eV}$ range for the same *soft excess* strength.

4 CAUSE OF EXTENDED STABLE REGION : HEATING AGENTS AND ION FRACTIONS

We have seen that the disk blackbody and the *soft excess* radiation at $\lesssim 0.5 \text{ keV}$ significantly influence the stability curve, implying that these components are important for shaping the ionic and thermal state of the WA (Section 3). Changes in the *disk blackbody* affect the low temperature arm ($\text{log } T \sim 4.5$) of the stability curve, whereas the *soft excess* influences the absorbing gas at $\text{log } T \sim 5.0 \text{ K}$. In this section we examine the important heating agents and the distribution of ion fractions of the signature ions in the WA along the stability curve. All the ionizing continua considered in this section are given by Equation 4. The effect of the thermal Comptonised *soft excess* gives the same qualitative results as the blackbody *soft excess* modeled by a blackbody (Equation 4, see).

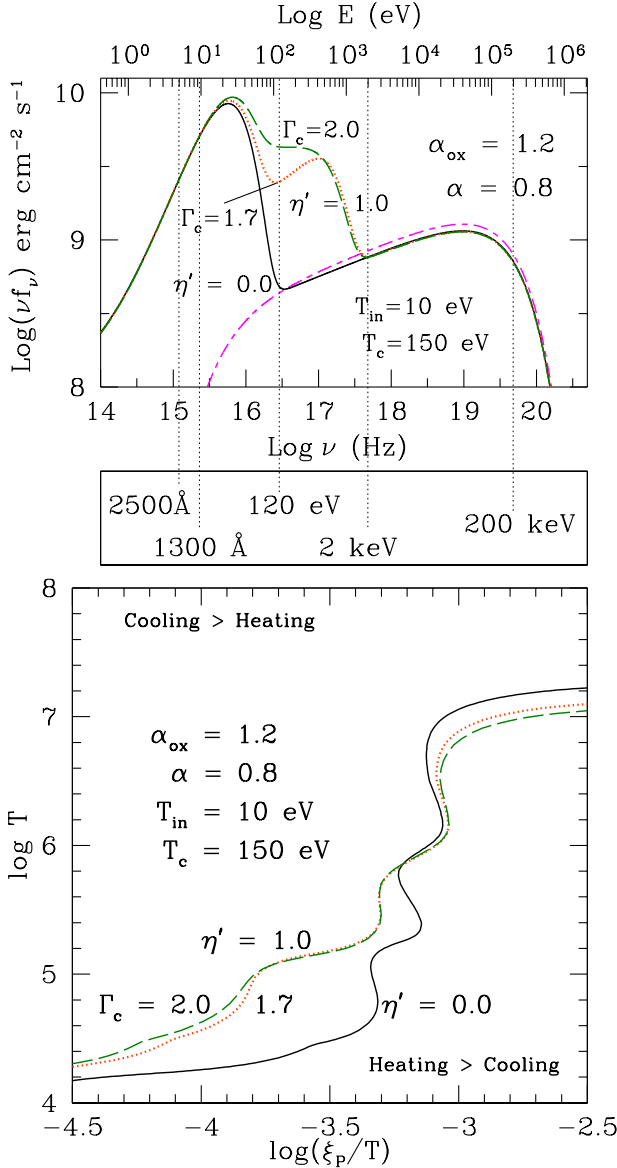


Figure 5. *Top panel* : Ionizing continua with *soft excess* component due to thermal Comptonisation given by Equation 5 with fixed values of $T_c = 150 \text{ eV}$, $T_{\text{in}} = 10 \text{ eV}$ and $\eta' = 1.0$. The different curves are for different values of Γ_c , namely 1.7 and 2.0. For comparison, we have also drawn the continuum with no *soft excess* (solid curve). With $\alpha = 0.8$ and $\alpha_{\text{OX}} = 1.2$, the accretion disk component and the X-ray power-law component are same for all the SEDs. The magenta, long-and-short-dashed curve is the same as in the top panels of Figures 3 and 4. We have included the energy values 1300 \AA and 120 eV to guide the eye in the context of observations of Mrk 478 (see text in Section 3.3.2) *Bottom panel* : The stability curves corresponding to the ionizing continua shown in the top panels.

4.1 Heating

CLOUDY works by dividing a gas into a set of thin concentric shells, referred to as ‘zones’ which have thicknesses that are small enough for the physical conditions across them to be nearly constant, maintained by continuously adjusting the physical thicknesses of these shells. For this sub-section, only, we have constrained the code to perform a single zone calculation for numerical convenience as we

are not concerned with quantitative rigor, but want to understand the qualitative trends.

Figure 6 shows the influence of these two components on the heating fraction ΔH of H^{+0} , He^{+1} , Fe and O as a function of ξ_P/T . All other ions and/or elements contribute less than 10% to ΔH .

On the left the solid and the dotted-and-dashed curves respectively correspond to a WA ionized by an SED with $T_{\text{in}} = 10$ and 30 eV (see Eqn 4). In both cases $\eta = 0$ so that there is no *soft excess* component in these SEDs, so any changes in the heating fractions are entirely due to the variation in the accretion disk spectrum.

On the right panels the solid and the dotted-and-dashed curves correspond to $\eta = 0$ and 3 respectively, while $T_{\text{in}} = 10 \text{ eV}$. Hence changes in the heating fractions in the right panels are due only to the varying strength of the *soft excess* component.

The top panels (labeled A) of Figure 6 show the region of the stability curves where the variation of these spectral components has maximum effect.

4.1.1 Hydrogen and Helium

Panels B and C of Figure 6 show the distribution of ΔH respectively for neutral Hydrogen H^{+0} and singly ionised Helium He^{+1} . In the left panels we see that there is no significant difference in the distributions as T_{in} increases from 10 to 30 eV . For both H^{+0} and He^{+1} , ΔH is considerably less for $\eta = 3.0$ than for $\eta = 0$ as seen in the right panels. Thus in either case (of the disk blackbody or the *soft excess*) H^{+0} and He^{+1} can be ruled out as the cause of extra heating causing the increase in the temperature of the stability curves in the range of $\log(\xi_P/T)$.

4.1.2 Iron

We find that in the disk blackbody and the *soft excess* cases the significant heating agents are the various species of iron. It is to be noted that the range of ΔH for Fe (panels D1, D2 & D3) is double that for O (panels E1, E2 & E3). The ΔH behaviour of the iron ions are affected, both, when we increase T_{in} from 10 to 30 eV , and when we increase η from 0 to 1. Fe^{+7} , Fe^{+8} , Fe^{+9} , Fe^{+10} and the Unresolved Transition Array (UTA, see below) are the most significant heating agents; and their contributions have been added to give the heating fraction due to iron (labeled ‘Iron’) in panels D1 through D3. On the left panels D2 and D3 the heating fractions of the individual ions of iron and the UTA are shown, respectively, for $T_{\text{in}} = 10$ and 30 eV . Similarly, the right panels D2 and D3 show ΔH for the individual iron ions and the UTA, respectively, for $\eta = 0$ and 3.0 . A WA which is overabundant in iron (Fields et al. 2005, 2007) and/or illuminated by a SED having photons facilitating absorption by iron will be warmer at relatively lower values of ξ_P . These two physical scenarios influence different ions of iron, which may help to distinguish between the otherwise degenerate effects.

For $-4.0 < \log(\xi_P/T) < -3.4$, where ΔH for iron is most affected by T_{in} , Fe^{+8} and Fe^{+9} are the dominant ions (panel D2 and D3 on the left of Figure 6). The ionization potentials for Fe^{+7} , Fe^{+8} , Fe^{+9} , and Fe^{+10} are 151.1, 235, 262.1 and 290.4 eV respectively. As the accretion disk becomes hotter, with T_{in} increasing from 10 to 30 eV , the number of photons with $E > 100 \text{ eV}$ increases by a factor of 27. It is this enhancement in the number of photons that influences these ions of iron differently in the two cases and hence changes the shape of the stability curves.

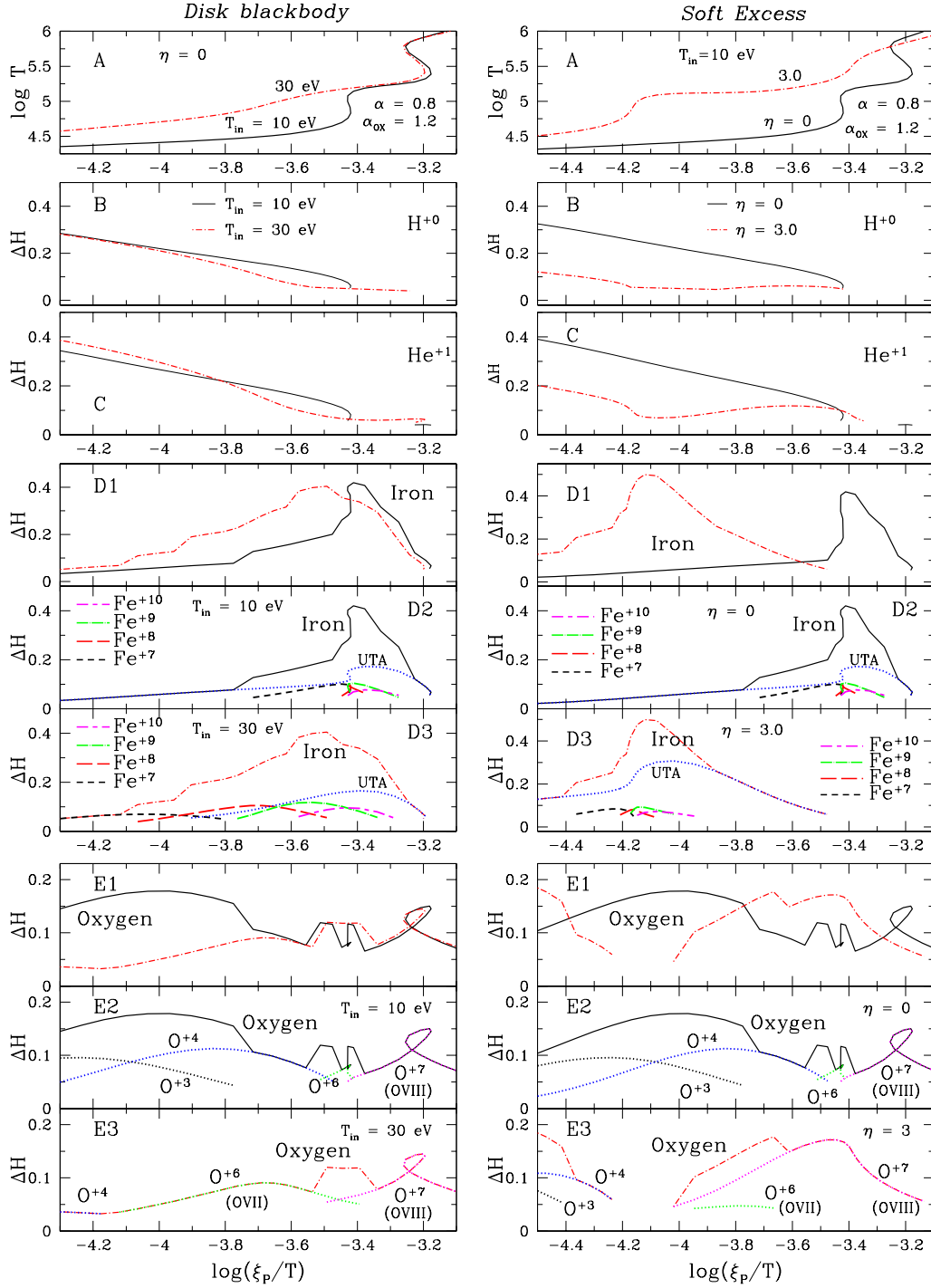


Figure 6. The principal heating agents which are being influenced by the soft spectral components *disk blackbody* (panels on the left) and *soft excess* (panels on the right) present in the SEDs of typical AGN. *Top panels (A)* : The stable part of the thermal equilibrium curves for an optically thin Solar metallicity gas illuminated by ionizing continua given by Equation 4. On the left panel the solid and the dotted-and-dashed lines correspond to SEDs having $T_{in} = 10$ and 30 eV respectively with $\eta = 0$ in both cases. The solid line in the right panel represents a SED with $\eta = 0$ and the dotted-and-dashed curve is for $\eta = 1.0$, where $T_{in} = 10$ eV for both the curves. We have zoomed in on the regions of the stability curves where they differ most from one to the other. The line schemes described for the left and right panels are maintained same for the lower panels in the figure. *Lower panels* : Fraction (ΔH) of the total heating caused by the various significant elements and ions. We have demonstrated the effects of all those elements which contribute $\gtrsim 10\%$ to the total heating in the same $\log(\xi_P/T)$ range as shown in the top panels. Panels B, C, D1 and E1 show the results for H^{+0} , He^{+1} , iron and oxygen respectively. The ‘break-up’ in heating fraction of iron are shown in panels D2 and D3 and the same for oxygen are shown in panels E2 and E3. Note that the y-range for the panels E1 through E3 for Oxygen are different from all other panels showing ΔH distributions because Oxygen never contributes more than 20% to the heating unlike other agents, some of which are responsible for even up to 50% of the heating for some values of $\log(\xi_P/T)$. Note that the discontinuity in the ΔH distribution of oxygen in the $\eta = 3.0$, $T_{in} = 10$ eV case (dotted-and-dashed curve in panels E1 and E3) is because the contribution drops below 5% for $-4.2 < \log(\xi_P/T) < 4.0$.

The UTA is a blend of the numerous absorption lines arising from the iron M-shell ions, $\text{Fe}^{+0} - \text{Fe}^{+15}$, due to their $n = 2-3$ (mainly 2p-3d, n being the principal quantum number of the active electron) transitions which are found to occur between 16 and 17 Å (730 - 776 eV) (Sako et al. 2001; Netzer 2004; Krongold et al. 2005a,b; Holczer et al. 2007, and reference therein). The energy ranges important for the UTA are likely to be influenced by the *soft excess* component of the SED. This effect is clearly seen by comparing the ΔH distributions of UTA in the right panels D2 and D3 of Figure 6; ΔH for iron is far more dominated by the UTA ΔH contribution for $\eta = 3.0$ case in the range $-4.4 < \log(\xi_P/T) < 3.6$.

Note that in panels D2 (both left and right), the solid curve for iron is multivalued at $-3.43 < \log(\xi_P/T) < -3.42$, just where the stability curve is multivalued (see panels A), giving multiple phases in pressure equilibrium. On the other hand, for the $T_{in} = 30$ eV and $\eta = 3$ curves (the dotted-and-dashed stability curves in panels A and the corresponding ΔH distribution of iron in panels D3, both left and right) there is no multivalued behaviour for $\log(\xi_P/T) \sim -3.4$. Thus the behaviour of the stability curve seems to be driven by the heating due to the different ions of iron.

4.1.3 Oxygen

Panels E1 through E3 show the results for the heating fractions contributed by Oxygen. Note the factor 2 smaller, y-range for the panels E1 through E3 because Oxygen never contributes more than 20% to the heating of the gas.

The left panels show that ΔH due to Oxygen is lower for $T_{in} = 30$ eV than that for $T_{in} = 10$ eV in the range $\log(\xi_P/T) \lesssim -3.6$. In the same range of $\log(\xi_P/T)$, the stability curve for $T_{in} = 30$ eV has higher temperature than the $T_{in} = 10$ eV curve (panel A on the left). Thus here Oxygen is not acting as one of the required heating agents resulting in a warmer absorber.

However, in the $\eta = 3.0$ case (right panels) Oxygen becomes a significant excess heating agent for $\log(\xi_P/T) > -3.6$ where the contributing ions are O^{+6} (OVII) and O^{+7} (OVIII).

As for iron, the ΔH distribution due to oxygen for the $T_{in} = 10$ eV, $\eta = 0$ case, are also multivalued at the same values, namely the narrow range $-3.43 < \log(\xi_P/T) < 3.42$ (panels E2, both left and right), although not as strongly as that for iron (panels D2, both left and right). Moreover, at $\log(\xi_P/T) \sim -3.4$, it is iron and not oxygen which is the dominant heating agent. However, oxygen is the dominant heating agent at higher values $\log(\xi_P/T) \sim -3.2$, and has multivalued ΔH distribution which drives the multi-phase nature of the solid stability curves at those values of $\log(\xi_P/T)$.

The ΔH distribution of oxygen for the $T_{in} = 30$ eV, $\eta = 0$ is shown in the left E3 panel (dotted-and-dashed curve). For $-3.8 < \log(\xi_P/T) \lesssim -3.3$ the oxygen ΔH is about 2 to 4 times lower than the iron ΔH (left panel D3). The oxygen ΔH dominates only beyond $\log(\xi_P/T) > -3.3$ where it is multivalued and is responsible for the multivalued nature of the stability curve (left panel A) at the same values of $\log(\xi_P/T)$.

For the $\eta = 3.0$, $T_{in} = 30$ eV case (right panel E3) as well, the oxygen ΔH contribution is lower than the iron ΔH (right panel D3) until $\log(\xi_P/T) \gtrsim -3.6$ beyond which the oxygen ΔH distribution determines the behaviour of the stability curve. Note that the stability curve (dotted-and-dashed in right panel A) is not multivalued at $\log(\xi_P/T) \gtrsim -3.6$ because the ΔH for oxygen is not multivalued.

Thus, at the higher ionization ($\log(\xi_P/T) \sim -3.2$) phase of

the WA, the nature of the stability curve seems to be driven by the heating due to the oxygen ions, predominantly O^{+7} (OVIII).

4.1.4 Zero oxygen and iron abundance

We have further illustrated the importance of iron and oxygen as the key players in determining the thermal properties of the WA using Figure 7. The distinction between the left and the right panels are as that in Figure 6; the upper panels being the same stability curves as in Figure 6 panels A, but for slightly different ranges of $\log(\xi_P/T)$ and wider ranges of $\log T$.

Comparing the stability curves for Solar metallicity gas (top panels), which have pronounced kinks in the temperature range $4.2 < \log T < 6.5$, with the relatively featureless ones for gas with zero O and Fe (bottom panels), we see that the detailed shape of the curves in the temperature range $\sim 4.2 < \log T < 6.5$ are governed by the atomic interactions due to oxygen and iron (also see Chakravorty et al. 2009). As a result, the SED induced differences between the solid and the dotted-and-dashed stability curves in the top panels are significantly smoothed out in the bottom panels.

For $-3.7 < \log(\xi_P/T) < -3.3$ the rise in temperature of the Solar metallicity stability curves in the top left panel shows a temperature difference of 0.4 dex from one curve to the other. This difference is reduced to 0.2 dex when iron and oxygen are not present in the gas (lower left panel) suggesting that a hotter accretion disk ($T_{in} = 30$ eV) mainly affects ions of iron and oxygen which results in a hotter WA.

The temperatures of the Solar metallicity stability curves in the top right panels are remarkably different, by ~ 1 dex, for $-4.2 < \log(\xi_P/T) < -3.3$. These differences are significantly reduced to 0.3 - 0.5 dex when iron and oxygen are removed from the gas (lower right panel). This indicates that atomic interactions due to these elements are affected by the strength of the *soft excess* component. Unlike the accretion disk case, however, the stability curves in the lower right panel retain some of their differences in WA temperatures suggesting that other elements have a role as heating agents in the *soft excess* case. The detailed investigation of this effect is beyond the scope of this paper, but will be attempted soon in our future publications.

4.2 Ion fraction

Absorption lines and edges of OVII, with ionisation potential (IP) of 0.74 keV, and OVIII, with IP of 0.87 keV, are often prominent signatures of the WA in soft X-ray spectra. Hence the column densities of these two ions are often considered as important observable parameters for WA states (see introduction for references). At higher values of ξ_P , absorption by various ions of silicon become important, e.g. Netzer et al. (2003) show that SiXIV (IP of 2.67 keV) has a significant column density corresponding to the high temperature component of the WA. We choose these three ions to study the variation of their ion fraction as a function of ξ_P as the spectral components change in the ionizing continuum.

The ion fraction $I(X^{+i})$ of the X^{+i} ion is the fraction of the total number of atoms of the element X which are in the i^{th} state of ionization. Thus,

$$I(X^{+i}) = \frac{N(X^{+i})}{f(X) N_H},$$

where $N(X^{+i})$ is the column density of the X^{+i} ion and $f(X) =$

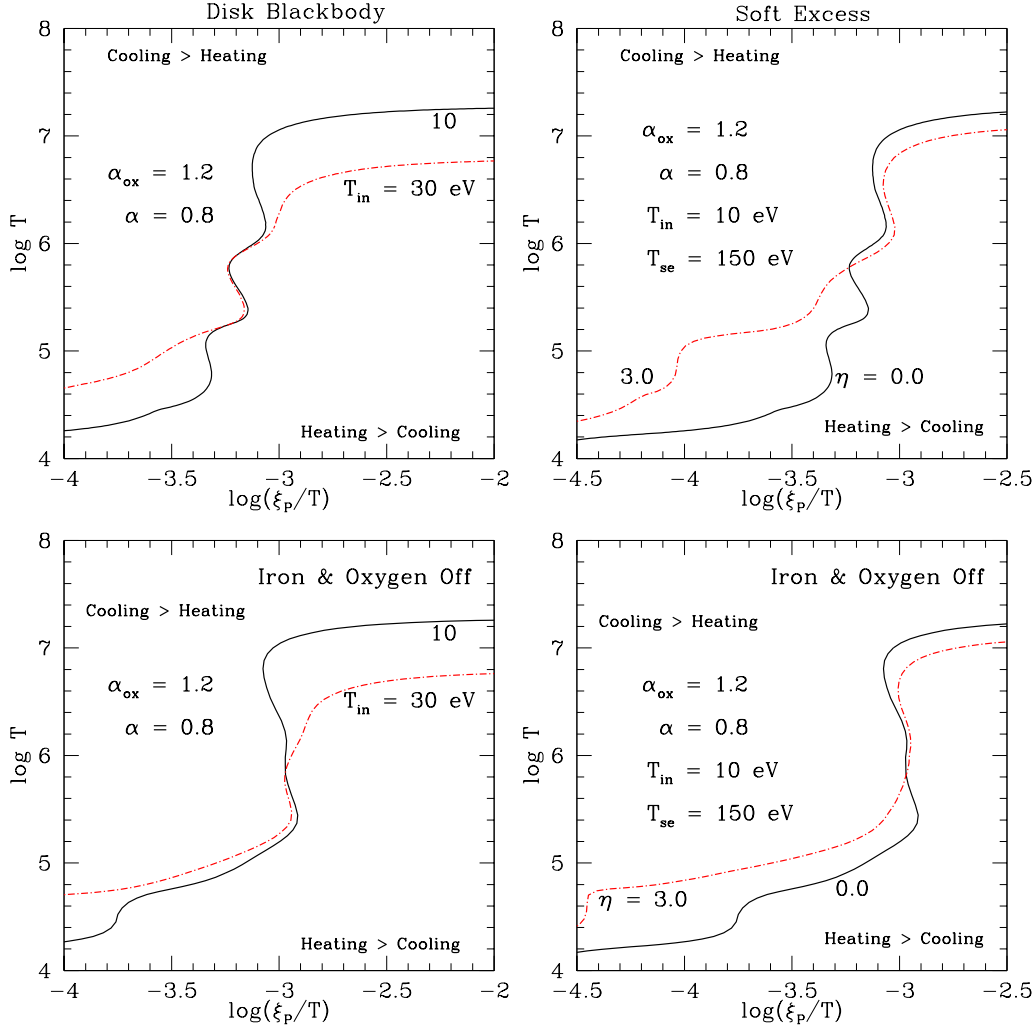


Figure 7. *Top Panels :* The comparison between the stability curves for Solar metallicity gas, when ionized by SEDs having accretion disks with different temperatures $T_{in} = 10$ and 30 eV (left) and when the ionizing continua have different strengths of the *soft excess* component $\eta = 0$ and 3.0 (right). *Bottom panels :* The same ionizing continua are used to illuminate a gas for which iron and oxygen have been removed. The relative differences in the stability curves are almost entirely removed in the lower left panel, and are significantly reduced in the lower right panel, indicating that these spectral components strongly influence the ions of iron and oxygen.

$n(X)/n_H$ is the ratio of the number density of the element X to that of hydrogen.

The top panels of Figure 8 show the distribution of $\log T$ with respect to $\log \xi_P$ for the stable WA phases. The gaps in the lines correspond to the range of ionization parameter over which the gas is thermally unstable. The lower panels show I(OVII), I(OVIII) and I(SiXIV).

As before, left panels in Figure 8 correspond to the changes in the diskblackbody. For $T_{in} = 10$ eV we can see three distinct regions of ξ_P separated by intermediate ranges of thermally unstable solutions. These regions are respectively dominated by OVII, OVIII and SiXIV. However, when T_{in} is raised to 30 eV, the stability curve becomes stable all the way up to $\log T = 5.3$ and the OVII dominated phase gradually merges in to the OVIII dominated gas, as demonstrated by the uninterrupted dotted-and dashed line in the top left panel. Thus there seems to be a continuous distribution of possible thermal solutions resulting from the greater production of OVII (second panel from top) which, in its turn, is a result of the enhanced number of $E \gtrsim 100$ eV photons coming from a hotter

accretion disk with $T_{in} = 30$ eV. The change in the shape of the *disk blackbody* does not change the ion fraction distribution of the high ionization species like OVIII or SiXIV (the two lowest panels) or the stability curve for $\log T > 5$ and $\log \xi_P > 1.7$. Thus the higher temperature ($\log T \gtrsim 5$) phase of the ionized absorber remains unaffected.

The effect of the *soft excess* component is demonstrated in the right panels of Figure 8. In this case the increase in the strength of the *soft excess* component from $\eta = 0$ to $\eta = 3.0$ makes the absorber thermally stable all the way up to temperatures of $\log T \sim 6$. The third panel from the top shows that increase in the strength of the *soft excess* component mainly influence the occurrence of OVIII. The fraction of OVII is reduced for $\eta = 3.0$ because of the facilitated production of OVIII at lower values of $\log \xi_P$. This is caused by increase in the number of ~ 100 eV – 2 keV photons by a factor of ~ 7.5 . The ion fraction distribution of SiXIV however, remains unaffected (bottom panel).

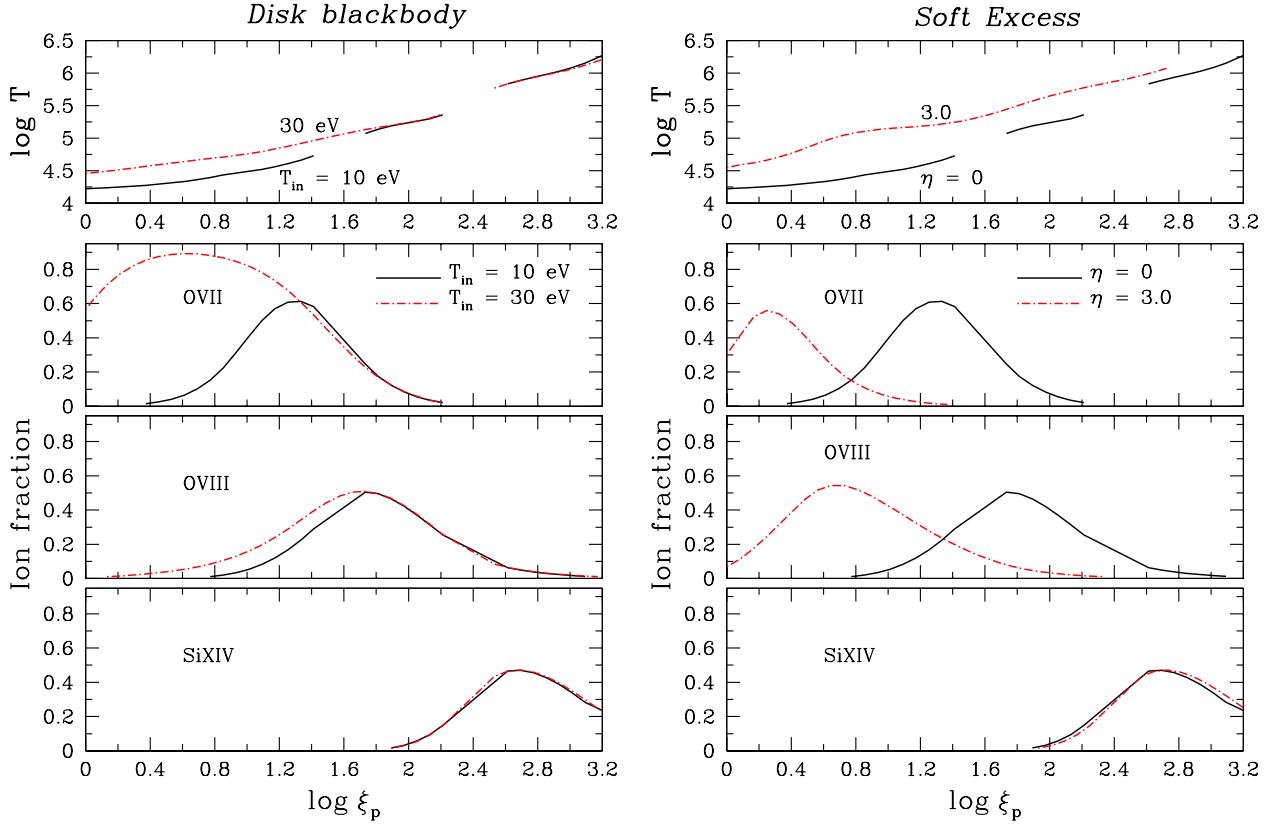


Figure 8. The ion fractions of some of the relevant ions as a function of ionization parameter; the left panels show how this distribution is influenced by the *disk blackbody* spectral component and the right panels show the same for the *soft excess*. *Top panels* : The distribution of temperature as a function of ξ_P is plotted for the thermally stable WA. The gaps in the curves correspond to the range of ξ_P over which the stability curve is thermally unstable. An increase in accretion disk temperature T_{in} from 10 to 30 eV makes the gas stable at $\log T \sim 5$. When the strength of the *soft excess* is increased from $\eta = 0$ to 3.0, all the phases of the WA become thermodynamically stable up to a temperature of $\log T \sim 6.3$. *Lower panels* : Ion fraction for various ions (as labeled) important for the WA states. The line-style scheme followed here is the same as in Figure 6 and is also labeled in the second panel from the top. See text for the physical implications of the ion fraction distribution.

5 OTHER SIGNIFICANT PHYSICAL PARAMETERS FROM EARLIER STUDIES

Chakravorty et al. (2009) had studied the properties of the WA as a function of the X-ray spectral index α and the chemical abundance of the gas. In this subsection we summarise some of those results which are relevant in the context of the soft spectral components of typical AGN continua and their effect on the WA.

5.1 X-ray spectral index α

Chakravorty et al. (2009, Section 5.1 and Figure 3) showed that there was no thermally stable absorber for $\log T > 4.4$ for a flat spectral index of $\alpha = 0.2$ (in Equation 2, $\alpha_{OX} = 1.2$). Figure 9 shows the stability curve using Equation 2 with $\alpha = 0.2$ (dotted, magenta line), which corresponds to an ionizing continuum with no *soft excess* component, shows no appreciable stable WA phase at $T \sim 10^5$ K. In Section 4 of this paper we have seen that the presence of *soft excess* component in the AGN spectra facilitates the existence of thermally stable gas at $\log T \sim 5.0$. However, throughout we have used $\alpha = 0.8$. It is thus crucial to check if the *soft excess* component can result in stable 10^5 K gas even if $\alpha \sim 0.2$.

The solid, the dotted-and-dashed and the dashed curves in Figure 9 show the comparison between the stability properties of the WA ionized by SEDs given by Equation 4 with $T_{se} = 150$ eV, $\eta = 3.0$ and $T_{in} = 10$ eV but various values of α (0.8, 0.5 and 0.2). The range, in $\log(\xi/T)$, of stable WA phase at $\log T \sim 5$ decreases as a function of decreasing value of α . However, even for α as low as 0.2 we still see a stable phase at $\log T \sim 5$. Thus the appearance of a stable state at $\log T \sim 5.0$ for the $\alpha = 0.2$ curve can be attributed to the presence of a strong *soft excess* component present in the ionizing continuum. However, if $\alpha \lesssim 0.2$, even with contributions from a strong *soft excess* component, there is no evidence for stable gas at any higher temperature than $\log T > 5.3$ (refer to the dashed, blue curve).

Notice that in Figure 9 the stability curves are drawn using ξ instead of ξ_P . The normalisation scheme for the ionisation parameter discussed in Section 3.1 is not appropriate while comparing SEDs with different values of the X-ray spectral index α .

5.2 Chemical abundance of the absorber

We discuss the role of the elemental abundances of the absorbing medium in Chakravorty et al. (2009). Here, we revisit the super-Solar metallicity results, but, with more realistic AGN continua

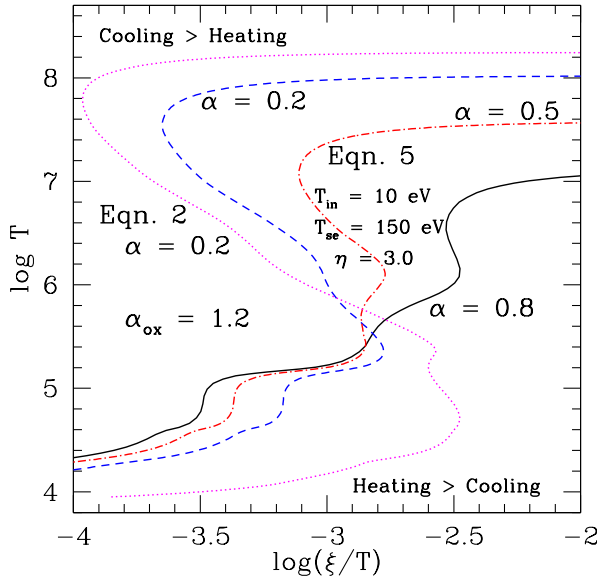


Figure 9. Thermal equilibrium curves generated using SEDs given by Equation 4 with a strong *soft excess* ($T_{se} = 150$ eV, $\eta = 3.0$ and $T_{in} = 10$ eV) for a range of X-ray slope $\alpha = 0.8$ 0.5 and 0.2 (respectively drawn with the solid, the dotted-and-dashed and the dashed lines). The stable phase at $\log T \sim 5.0$ the range of $\log(\xi/T)$ progressively decreases as α decreases from 0.8, to 0.5 and then to 0.2. For comparison we have used Equation 2 with $\alpha = 0.2$, which corresponds to an ionizing continuum which has no *soft excess* component, and drawn the dotted stability curve which is consistent with no stable WA phase at $\log T \sim 5.0$.

given by Equation 4 ($\alpha = 0.8$, $\eta = 3.0$ and $T_{in} = 10$ eV). The stability curves are shown in Figure 10 for WA abundances from Solar (Z_{\odot}) to $9 Z_{\odot}$ in steps of 2. The qualitative results are the same as in Chakravorty et al. (2009).

On the low temperature ($\log T \lesssim 4.5$, corresponding to OVII like ions) arm of the stability curves, super-Solar metallicity results in a cooler absorber for the same ξ_P (or ξ) values, with an increase in the range of ξ_P over which we get stable WA. Thus super-Solar metallicity opposes the role of increased T_{in} (see Figure 3 in Section 3.2).

For the intermediate temperature arm of the stability curve ($\log T \sim 5.0$, corresponding to OVIII like ions) super-Solar abundance decreases the range of stable WA, thus opposing the influence of the increase in η in the ionizing continuum (see Figure 4 in Section 4).

On the highest temperature arm of the WA ($\log T \sim 6.0$, corresponding to SiXIV like ions) super-Solar gas tends to be hotter, and is thermodynamically stable for a larger range of values of $\log(\xi_P/T)$. Thus the fine tuning of ξ_P values to detect such species of ions is relaxed if the absorber has super-Solar abundance, and the probability of detecting these high ionization species is increased. In this regime, the influence of high metallicity is degenerate with the influence of increasing α in the ionizing continuum, but only if $\alpha \gtrsim 0.8$ (see Figure 9 in Section 5.1).

6 MULTI-PHASES WARM ABSORBER

The stability curves we have derived in the previous sections often contain segments that allow phases at different temperatures to

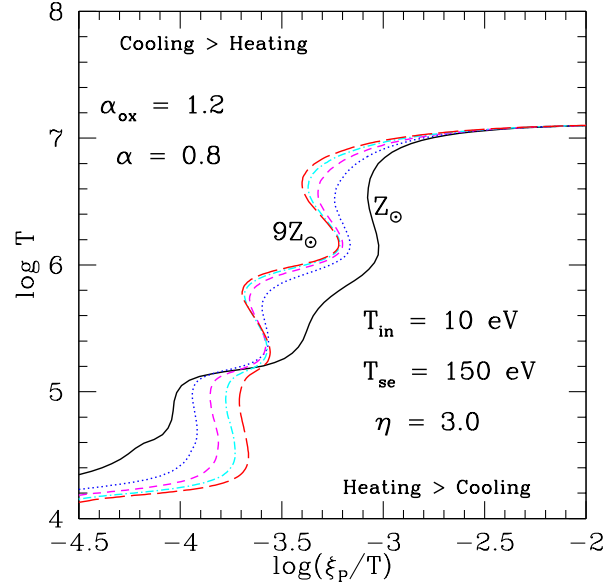


Figure 10. Stability curves for absorbers with Solar and super-Solar abundance from Z_{\odot} to $9 Z_{\odot}$ in steps of 2. The ionizing continuum has a strong *soft excess* (Equation 4 with : $\alpha = 0.8$, $\eta = 3.0$ and $T_{in} = 10$ eV).

occur at similar pressure ξ_P/T indicating the possibility of two or more distinct WA phases within the same medium to exist at near pressure equilibrium. However, variations in some of the physical parameters can also result in the possibility of multi-phase absorbers being lost.

Observationally, distinct phases in pressure equilibrium have been derived in a number of cases of WAs (Krongold et al. 2003; Netzer et al. 2003; Chelouche & Netzer 2005; Krongold et al. 2007; Andrade-Velazquez et al. 2010), while in other cases it has been claimed that there is a continuous range of ionization parameter (Ogle et al. 2004; Steenbrugge et al. 2005). Since a wide range of physical parameters have been studied in this paper and Chakravorty et al. (2009) for their effects on the WA, we can now form a clearer picture of which physical conditions favour the multi-phase absorbers.

The *disk blackbody* component from the accretion disk affects the lower temperature part of the stability curve (Sections 3 and 4). Figure 3 shows that the stability curve (solid line) with $T_{in} = 10$ eV has a slim range $-3.34 \leq \log(\xi_P/T) \leq -3.31$ over which gas at low temperatures $\log T \lesssim 4.3$ can be in pressure equilibrium with the absorber at intermediate temperatures $\log T \lesssim 5.0$. However, as T_{in} is increased, all possibilities of such multi-phase structure is lost, instead the curve becomes stable in the intermediate temperature range supporting a continuous distribution of allowed pressure and temperature in this phase space. Thus cooler accretion disks support a multi-phase WA, although for a narrow range of pressure.

An ionizing continuum having no *soft excess* (solid line in Figures 4 and 5) allows for a multi-phase between $\log T \sim 5$ and 6. However, with the increase in the strength of the *soft excess* component the range of $\log(\xi_P/T)$ over which the possibility of multi-phase exists reduces from 0.09 dex for $\eta = 0$ to 0.006 dex for $\eta = 1.0$ and to 0 for $\eta = 3.0$.

Chakravorty et al. (2009) had emphasised that super-Solar abundances increase the range of $\log(\xi/T)$ with the possibility

of multi-phase WA (also see Komossa & Mathur 2001). For example, as the metallicity of the gas was increased from 1.0 to 3.0 to 5.0, $\Delta_{45}[\log(\xi/T)]$ increased from 0.012 to 0.08 to 0.1, where $\Delta_{45}[\log(\xi/T)]$ gives the range of common values of $\log(\xi/T)$ over which the WA has stable phases at both $\sim 10^5$ and $\sim 10^4$ K. Beyond a metallicity of $5Z_{\odot}$, $\Delta_{45}[\log(\xi/T)]$ was found to drop because the range of $\log(\xi/T)$ for the $\sim 10^5$ WA was found to decrease with the increase in metallicity and became zero for a gas with metallicity $9Z_{\odot}$.

Similar trends are retained for the continua in this paper. As the metallicity of the gas is increased, keeping the ionizing continuum the same, the stable phases increasingly align along the same values of $\log(\xi_P/T)$ (Figure 10), strongly suggesting the presence of multi-phase WA. $\Delta_{45}[\log(\xi_P/T)]$ increases from 0 to 0.02 to 0.04 to 0.045 as metallicity is increased from Solar to 3, 5 and 7 times Solar. Beyond this high metallicity, $\Delta_{45}[\log(\xi_P/T)]$ becomes constant. There is a even more significant increase in $\Delta_{56}[\log(\xi_P/T)]$ from 0 to 0.03 to 0.08 to 0.11 to 0.13 with the increase in metallicity from Solar to 3, 5, 7 and 9 times Solar.

For NGC 3783, Netzer et al. (2003) found three distinct phases of the WA in near pressure equilibrium. In Figure 10 we see that only for $Z = 9Z_{\odot}$ there is a very narrow range of 0.03 dex in which all three phases of the WA, at temperatures $\sim 10^4, 10^5$ and 10^6 K, are stable in the range $-3.69 \leq \log(\xi_P/T) \leq -3.66$. Interestingly, the stability curve for a much lower metallicity, $Z = 5Z_{\odot}$, gas but ionized by a continuum with weaker *soft excess* ($\eta = 1.0$, not shown in Figure 10) shows the three phases in pressure equilibrium for a larger range of 0.08 dex for $-3.48 \leq \log(\xi_P/T) \leq -3.4$. Thus, it is easier (relatively lower super-Solar metallicity) to have 3 phases in pressure equilibrium if the strength of the *soft excess* is lower. In all the physical conditions of the WA, that were studied by Chakravorty et al. (2009), three phases of the WA were found to coexist in pressure equilibrium for still lower metallicity $\gtrsim 3Z_{\odot}$ which brings it down to observed values (e.g. see Fields et al. 2005, 2007, for MRK 279). It is to be noted, however, that the continua used by Chakravorty et al. (2009) had no *soft excess* component in them.

7 CONCLUSION

We have examined the effect of spectral energy distributions including hot disks and *soft excess* spectral components in the energy ‘blind spot’ between 13 - 100 eV (Equations 4 and 5) on warm absorber. We investigated whether the spectral shapes can, in turn, be constrained from the observed properties of the warm absorber.

We summarise our results as follows :

- The maximum temperature of the accretion disk component (see Equation 4, Section 2.2) strongly affects on the low temperature ($\log T \lesssim 4.5$) arm of the stability curve, the thermal properties of which are largely decided by ions Fe^{+7} to Fe^{+10} and O^{+6} (OVII). This phase of the WA becomes hotter and thermodynamically stable over a larger range of ξ when the ionising continuum is hotter ($T_{in} = 30$ eV) compared to $T_{in} = 10$ eV. Thus hotter accretion disks are more likely to produce WA phases characterised by ions having similar ionisation potentials to OVII. However, the possibility of this phase of the WA being in pressure equilibrium with the higher temperature phases is eliminated in the hot disk cases as $\Delta_{45}[\log(\xi/T)]$ decreases from 0.03 for $T_{in} = 10$ eV to 0 for $T_{in} = 20$ and 30 eV. Changes in the accretion disk temperature however, do not affect the higher temperature arms of the stability curve.

- The thermal properties of the intermediate temperature ($\log T \sim 5.0$) branch of the stability curve are essentially determined by atomic interactions due to the different ions of iron and OVIII (IP = 0.87 keV). We find that with the increase in the relative strength η of the *soft excess* component this 10^5 K stable phase of the WA spans a much larger range of $\log(\xi/T)$ (by 0.4 dex from $\eta = 0$ to $\eta = 3.0$) thus increasing the probability of finding WA phases characterised by ‘OVIII like’ ions.

- For a gas whose chemical composition is devoid of iron and oxygen, changes in the accretion disk spectral component bring about no change in the properties of the WA, and changes due to the variation in the strength of the *soft excess* component are significantly reduced.

- The highest temperature arm ($\log T \sim 6.0$) of the stability curve which is characterised by the ions having similar IP to that of SiXIV (IP = 2.67 keV), is left almost unaffected by any changes either in the accretion disk component or in the *soft excess* component.

- An AGN continuum with a flat X-ray slope will not produce high IP ions like SiXIV, and may show signatures of lower IP ions like OVIII (IP = 0.87 keV) only if a sufficiently strong *soft excess* component is present in the SED.

- The metallicity of the gas plays an important role in determining the multi-phase nature of the warm absorber. The possibility of the 10^4 and the 10^5 K phases of the warm absorber occurring at similar values of $\log(\xi/T)$ is increased if the absorber is super-Solar in abundance. Similarly, the chances of having pressure equilibrium between the 10^5 and the 10^6 K phases are also increased by the super-Solar metallicity of the gas. However, all three phases, together, are found to be in pressure equilibrium only if $Z > 3Z_{\odot}$, and the required abundance to achieve this is increased if the ionizing continuum has stronger *soft excess*.

ACKNOWLEDGEMENTS

SC sincerely thanks Profs. Andy Fabian and Hagai Netzer for providing valuable suggestions in the early stage of preparing this paper.

REFERENCES

- Allende Prieto, C., Lambert, D.L., & Asplund, M., 2001, ApJ, 556, L63
- Allende Prieto, C., Lambert, D.L., & Asplund, M., 2002, ApJ, 573, L137
- Andrade-Velazquez, M.; Krongold, Y.; Elvis, M.; Nicastro, F.; Brickhouse, N.; Binette, L.; Mathur, S.; Jimenez-Bailon, E. 2010, ApJ, 711, 888
- Arnaud, K. A. 1996, ASPC, 101, 17
- Bechtold, J. et al. 1994, AJ, 108, 759
- Behar, E. 2009, ApJ, 703, 1346
- Beloborodov, A.M. 1999, ASPC, 161, 295.
- Blustin, A. J. et al. 2003, A&A, 403, 481
- Brinkmann, W. 1992, A&A, 254, 460
- Buehler, P.; Courvoisier, T. J.-L.; Staubert, R.; Brunner, H.; Lamer, G. 1995, A&A, 295, 309
- Chakravorty, S., Kembhavi, A.K., Elvis, M., Ferland, G. & Badnell, N.R., 2008, MNRAS, 384L, 24
- Chakravorty, S., Kembhavi, A.K., Elvis, M. & Ferland, G., 2009, MNRAS, 393, 83

- Chelouche, D., Netzer, H. 2005, *ApJ*, 625, 95
- Collinge, M. J. et al. 2001, *ApJ*, 557, 2
- Coppi, P.S. 1992, *MNRAS*, 258, 657
- Coppi, P.S. 1999, *ASPC*, 161, 375
- Crummy, J.; Fabian, A.C.; Gallo, L.; Ross, R. 2006, *MNRAS*, 365, 1067
- Czerny, B.; Elvis, M., 1987, *ApJ*, 321, 305.
- Elvis, M.; Wilkes, B. J.; Tananbaum, H., 1985, *ApJ*, 292, 357
- Elvis, M.; Green, R. F.; Bechtold, J.; Schmidt, M.; Neugebauer, G.; Soifer, B. T.; Matthews, K.; Fabbiano, G., 1986, *ApJ*, 310, 291.
- Elvis, M. et al. 1994, *ApJS*, 95, 1
- Fields, D. L.; Mathur, S.; Pogge, R.; Nicastro, F.; Komossa, S.; Krongold, Y. 2005, *ApJ*, 634, 928
- Fields, D. L.; Mathur, S.; Krongold, Y.; Williams, R.; Nicastro, F. 2007, *ApJ*, 666, 828
- Frank, J., King, A., & Raine, D. 2002, *Accretion Power in Astrophysics* (3rd ed.; Cambridge: Cambridge Univ. Press)
- Gehrels, N and Williams, E.D. 1993, *ApJ*, 418L, 25
- George, I. M.; Turner, T. J.; Netzer, Hagai; Nandra, K.; Mushotzky, R. F. & Yaqoob, T., 1998, *ApJS*, 114, 73
- Gierlinski M.; Done C. 2004, *MNRAS*, 349L, 7
- Gondhalekar, P. M.; Kellett, B. J.; Pounds, K. A.; Matthews, L.; Quenby, J. J., 1994, *MNRAS*, 268, 973
- Green, P.J. et al. 2009, *ApJ*, 690, 644
- Grevesse, N., & Sauval, A.J., 1998, *Space Science Review*, 85, 161
- Grupe, D.; Mathur, S.; Wilkes, B. & Osmer, P., 2006, *AJ*, 131, 55
- Haardt, F.; Maraschi, L. 1993, *ApJ*, 413, 507
- Halpern, J.P., 1984, *ApJ*, 281, 90
- Hess, C.J.; Kahn, S.M.; Paerels, F.B.S., 1997, *ApJ*, 478, 94
- Holczer, T.; Behar, E.; Kaspi, S. 2007, *ApJ*, 663, 799
- Holweger, H., 2001, Joint SOHO/ACE workshop “Solar and Galactic Composition”. Edited by Robert F. Wimmer-Schweingruber. Publisher: American Institute of Physics Conference proceedings, 598, 23
- Kaastra, J. S.; Steenbrugge, K. C.; Raassen, A. J. J.; van der Meer, R. L. J.; Brinkman, A. C.; Liedahl, D. A.; Behar, E. & de Rosa, A., 2002, *A&A*, 386, 427
- Kinkhabwala, A. et al. 2002, *ApJ*, 575, 732
- Komossa, S. & Meerschweinchen, J. 2000, *A&A*, 354, 411
- Komossa, S. & Mathur 2001, *A&A*, 374, 914
- Korista, K.; Ferland, G.; Baldwin, J., 1997, *ApJ*, 487, 555.
- Krolik, J. H., McKee, C. F., & Tarter, C. B. 1981, *ApJ*, 249, 422
- Krolik, J., & Kriss, G. A., 2001, *ApJ* 561, 684
- Krongold, Y.; Nicastro, F.; Brickhouse, N. S.; Elvis, M.; Liedahl, D. A. & Mathur, S., 2003, *ApJ* 597, 832
- Krongold, Y.; Nicastro, F.; Elvis, M.; Brickhouse, N. S.; Mathur, S. & Zezas, A., 2005a, *ApJ* 620, 165
- Krongold, Y.; Nicastro, F.; Brickhouse, N. S.; Elvis, M. & Mathur, S., 2005b, *ApJ* 622, 842
- Krongold, Y.; Nicastro, F.; Elvis, M.; Brickhouse, N.; Binette, L.; Mathur, S.; Jiménez-Bailón, E., 2007, *ApJ*, 659, 1022
- Laor, A., 1990, *MNRAS*, 246, 369.
- Laor, A.; Fiore, F.; Elvis, M.; Wilkes, B.J.; McDowell, J.C., 1997, *ApJ*, 477, 93
- Lightman, A. P., & Zdziarski, A. A. 1987, *ApJ*, 319, 643.
- Lynden-Bell, D., 1969, *Natur*, 223, 690
- Lopez, L. A.; Brandt, W. N.; Vignali, C.; Schneider, D. P.; Chartas, G.; Garmire, G. P. 2006, *AJ*, 131, 1914
- Makishima, K.; Maejima, Y.; Mitsuda, K.; Bradt, H. V.; Remillard, R. A.; Tuohy, I. R.; Hoshi, R.; Nakagawa, M. 1986, *ApJ*, 308, 635.
- Malkan, M. A.; Sargent, W. L. W., 1982, *ApJ*, 254, 22.
- Marshall, H. L.; Carone, T. E.; Shull, J. Michael; Malkan, M. A.; Elvis, M., 1996, *ApJ*, 457, 169
- Mathews, W.G.; Ferland, G.J., 1987, *ApJ*, 323, 456
- Matsumoto, C.; Leighly, K. M.; Marshall, H. L., 2004, *ApJ*, 603, 456
- Mitsuda, K. et al. 1984, *PASJ*, 36, 741
- Nandra, K. & Pounds, K. A. 1994, *MNRAS*, 268, 405
- Netzer, H. 1985, *MNRAS* 216, 63
- Netzer, H. 1987, *MNRAS*, 225, 55
- Netzer, H. 1993, *ApJ*, 411, 594
- Netzer et al. , 2003, *ApJ* 599, 933
- Netzer, H. 2004, *ApJ*, 604, 551
- Neugebauer, G.; Oke, J. B.; Becklin, E. E.; Matthews, K. 1979, *ApJ*, 230, 79.
- Ogle, P. M., Mason, K. O., Page, M. J., Salvi, N. J., Cordova, F. A., McHardy, I. M. & Priedhorsky, W. C. 2004, *ApJ*, 606, 151
- Page, K. L.; Reeves, J. N.; O’Brien, P. T.; Turner, M. J. L.; Worrall, D. M. 2004, *MNRAS*, 353, 133
- Page, K. L.; Schartel, N.; Turner, M. J. L.; O’Brien, P. T. 2004, *MNRAS*, 352, 523
- Piconcelli, E.; Jimenez-Bailon, E.; Guainazzi, M.; Schartel, N.; Rodriguez-Pascual, P. M.; Santos-Lleo, M. 2005, *A&A*, 432, 835.
- Porquet, D.; Reeves, J. N.; O’Brien, P.; Brinkmann, W. 2004, *A&A*, 422, 85
- Pounds, K.; Reeves, J. 2002, *astro-ph/0201436*
- Pringle, J. E.; Rees, M. J.; Pacholczyk, A. G., 1973, *A&A*, 29, 179
- Reynolds, C.S. & Fabian, A.C., 1995, *MNRAS*, 273, 1167
- Reynolds, C. S. 1997, *MNRAS*, 286, 513
- Ross, R. R.; Fabian, A. C. 1993, *MNRAS*, 261, 74
- Ross, R. R.; Fabian, A. C. 2005, *MNRAS*, 358, 211
- Rybicki G. B., Lightman A. P., 1986, *Radiative Processes in Astrophysics* (New York : John Wiley & Sons Inc.)
- Sako, M. et al. 2001, *A&A*, 365L, 168
- Shakura, N. I.; Sunyaev, R. A. 1973, *A&A*, 24, 337
- Shang, Z. et al. 2005, *ApJ*, 619, 41
- Shields, G. A. 1978 *Nature*, 272, 706.
- Siemiginowska, A.; Kuhn, O.; Elvis, M.; Fiore, F.; McDowell, J.; Wilkes, B. J. 1995, *ApJ*, 454, 77.
- Sobolewska, M. A.; Siemiginowska, A.; Zycki, P. T., 2004a, *ApJ*, 608, 80.
- Sobolewska, M. A.; Siemiginowska, A.; Zycki, P. T., 2004b, *ApJ*, 617, 102.
- Stalin, C. S.; Petitjean, Patrick; Srianand, R.; Fox, A. J.; Coppolani, F.; Schwope, A. 2010, *MNRAS*, 401, 294
- Steenbrugge, K.C. et al. 2005, *A&A* 434, 569
- Tananbaum, H. et al. 1979, *ApJ*, 234L, 9
- Tueller, J.; Mushotzky, R. F.; Barthelmy, S.; Cannizzo, J. K.; Gehrels, N.; Markwardt, C. B.; Skinner, G. K. & Winter, L. M., 2008, *ApJ*, 681, 113
- Turner, A. K., Fabian, A. C., Lee, J. C., & Vaughan, S. 2004, *MNRAS*, 353, 319
- Vignali, C.; Brandt, W. N.; Boller, T.; Fabian, A. C.; Vaughan, S., 2004, *MNRAS*, 347, 854
- Wilkes, B.J. & Elvis, M., 1987, *ApJ*, 323, 243
- Zdziarski, A. A.; Johnson, W. N.; Magdziarz, P. 1996, *MNRAS*, 283, 193
- Zheng, W.; Kriss, G.A.; Telfer, R.C.; Grimes, J.P. & Davidsen, A.F., 1997, *ApJ*, 475, 469

Zycki, P. T.; Done, C.; Smith, D. A. 1999, MNRAS 309, 561